Rock Mechanics: Meeting Society's Challenges and Demands – Eberhardt, Stead & Morrison (eds)
© 2007 Taylor & Francis Group, London, ISBN 978-0-415-44401-9

Numerical modeling approach of failure modes for cemented backfill sill mats

C. Caceres, R. Pakalnis & P. Hughes
Norman B. Keevil Institute of Mining Engineering, University of British Columbia, Vancouver, BC, Canada

T. Brady
Spokane Research Laboratory, NIOSH

ABSTRACT: Cemented backfill sill mats are an artificial pillar used to improve recovery by replacing an ore pillar by an artificial equivalent. In the design of a sill mat pillar, one should account for the driving forces in terms of the self weight of the sill mat plus the load of unconsolidated backfill used to fill the mined stope above it that results upon undermining the sill mat below. The resisting forces are largely governed by the strength properties of the cemented sill mat. This paper presents stability charts derived using numerical codes incorporating variable stope dip angles, sill mat thicknesses and strength properties of the cemented backfill and relating the results to limit equilibrium analytical equations presently in use.

1 INTRODUCTION

A cemented rockfill sill mat design should optimize the materials' requirements to achieve a stable condition, while meeting safety guidelines and minimizing mining costs.

This optimum is mainly driven by the cement cost which is the largest material cost component of backfill. Therefore, strategies intended at reducing cement content are of the highest benefit to mining operations. This paper defines and compares the relevant analytical relationships and numerical modeling results of backfill behavior on sill mat stability. The analysis is done via observations of practitioners and researchers working in the mining field.

2 LOAD OF BACKFILL

One of the key factors in assessing cemented rockfill (CRF) stability is quantifying the vertical stress acting on the top of the sill mat. *In situ* measurements and analytical derivations by numerous authors imply that arching of unconsolidated rockfill (URF) material decreases the vertical load on the sill by transferring part of the total vertical load to either rock walls. Methods to reliably determine the true load lead to more reliable and cost effective solutions in the design of sill mats. Overestimation of the vertical load produces unnecessary expense by increasing the quantity of cement used and/or the height of the sill mat required to withstand the estimated load. Underestimating can cause a premature failure of the sill mat while mining underneath, resulting in ore lost, ore dilution, cycle interruption, damage to equipment, and a compromise in personal safety.

3 STABILITY OF CEMENTED ROCKFILL SILL MATS

3.1 *Introduction*

There are five main modes of failure that should be analyzed to assess the stability of sill mats. These are caving, crushing, sliding, flexural, and rotational.

The degree of importance, in terms of an increase in the factor of safety, is related to the geometry of the stope and the height of the sill mat considering a fix percentage of cement (strength properties of the sill mat). Crushing is due to factors such as high degree of wall convergence and is not analyzed in the paper.

The stability of rockfill sill mats depends on two principal factors sill mat strength; and weight of backfill plus self weight of sill mat. Figure 1 shows stope geometry, strength, stress components, and failure modes in a sill mat pillar.

3.2 *Sill mat strength*

The strength of rockfill material can be substantially improved by the addition of a binding material. The

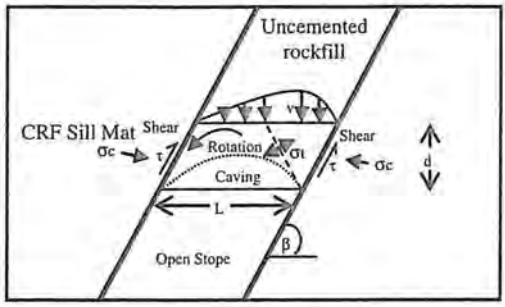

Figure 1. Geometry, strength and stress component and failure modes in a sill mat pillar.

improvement of CRF over URF comes on the shear and tensile strength components. Cement bonds that form between fill particles introduce cohesive and tensile strength absent in URF fills as well as an increment in the frictional component which is lower in URF fills.

The following two soil components directly determine backfill strength:

- frictional forces, proportional to the internal angle of friction (ϕ) of the aggregate material resulting from interlocking solid particles; and
- Portland cement (or similar soil binder) which significantly increases actual fill cohesion and tensile strength by binding the solid particles to each other.

The elastic modulus of backfill increases with the addition of cement. Literature and lab data confirm that CRF backfill has low modulus of elasticity ranging approximately from 100 MPa to 1000 MPa, and is normally one to two orders of magnitude less stiff than the surrounding rock.

3.3 *Backfill load*

This load is dependent upon the backfill properties: density and friction angle; and the geometry of the stope which includes the height of backfill material, span of the stope, and stope dip. A backfilled stope of infinite height will transfer only a portion of the total vertical load to a sill mat pillar – beyond a certain maximum height of backfill, the rest of the load is transfer to the stope walls due to an arching effect of the URF material.

4 NUMERICAL MODELLING OF SILL MATS USING FLAC2D

4.1 *Model construction*

A series of models are run to obtain design curves representing sill mat failure modes. These parametric studies account for variation in sill mat strength resulting from variations in cohesion, and stope geometry (span, and dip angle). In the interest of time efficiency, in all cases, a constant value of 410 kPa of vertical stress acting on top of the sill mat pillar was considered for the URF fills. This value has been estimated using numerical modeling for a vertical stope of 10 meter span and 35 meter rockfill height acting along the entire stope span. The distribution of the vertical stress along the stope span is *not* constant, and decreases with stope dip. However, this assumption of a constant vertical stress of 410 kPa yields an extra factor of safety in the sill mat pillar design.

The sill pillar thickness (height) for a given stope span vary according to the CRF strength properties. For this reason, the FLAC2D code conceived, automatically generates the grid and interfaces along the hanging and footwall to a specified pillar dimensions (height and span). Also, the number of grid elements per square meter is specified. The stable pillar dimensions result from a trial and error execution of the model with given strength properties.

An important consideration of the models is the interface elements designed to simulate distinct planes along which slip and/or separation can occur. Once the grid is constructed, material properties must be assigned to the individual grid elements. Elastic host rock properties are assigned to the outer grid elements. *In situ* host rock properties are obtained form intact rock cores (i.e., laboratory testing) and results are subsequently scaled to the *in situ* properties.

For the elastic model, the relevant properties are: density; bulk modulus; and shear modulus.

4.2 *Constitutive equations – Mohr Coulomb strain softening*

Swan & Brummer (2001) analyzed a strain softening model where a cohesive sill will lose integrity at a plastic strain of 1.5%. The CRF sill mat properties assigned on this paper are of a Mohr-Coulomb type of material with strain-softening behavior that lose its cohesion, and tensile strength, from the given value to zero (MPa), at a plastic strain of 1.5%. The friction angle falls from the original value of 37 degrees (at a plastic strain of 0%) to 15 degrees (at a plastic strain of 1.5%). At a plastic strain of 1.5%, cohesion will be zero but there is still some strength because of the friction angle. For the Mohr-Coulomb plasticity model, the relevant properties are density, bulk modulus, shear modulus, friction angle, cohesion, dilation angle, and tensile strength. Figure 2 illustrates an example of a strain-softening model for the cohesion strength parameter.

4.3 *Model execution*

For a given value of cohesion, span, and dip of the stope, the maximum height of the CRF sill pillar that

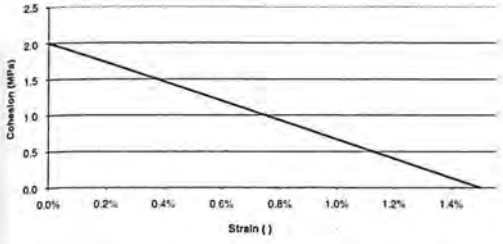

Figure 2. Strain softening model – cohesion example.

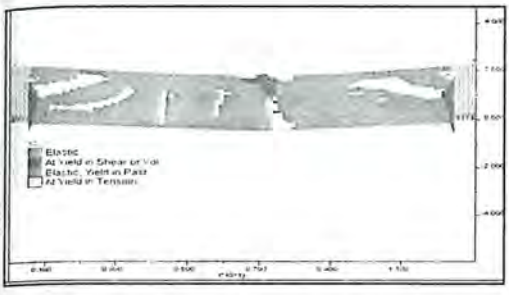

Figure 3. Sill mat flexural failure mode – plasticity state.

results in failure can be determined by trial and error. The stable sill pillar height was found when no more than 25 centimeters separate the stable and unstable conditions. The height determined this way results in a factor of safety of at least 1.0. In this case, 25 centimeters is arbitrarily determined, yet this choice represents an efficient compromise between the accuracy of a lower value (time consuming) and the time saved in using a higher value (which yields inaccuracy). Finally, the model automatically determines the most likely failure mode that could occur among flexural, rotational or sliding based on the fill properties and the geometry of the stope specified.

5 SILL MAT FAILURE MODES

5.1 *Flexural failure*

Figure 3 shows a thin sill pillar failing as a result of bending. It is evident that the top grid elements fail in compression, and that tension cracks form on the floor of the pillar, subsequently causing its collapse. Plasticity indicators are included. These identify the type of failure, e.g., shear failure or tensile failure, and whether the stress state in the zone is currently at yield, or has previously reached the yield surface but is currently below the yield surface ("at yield in past"). Also, for each type of failure mode, the analytical equation derived by Mitchell (1991) is shown.

$$\left(\frac{L}{d}\right)^2 > \frac{2\cdot(\sigma_t+\sigma_c)}{\sigma_v+d\cdot\gamma} \qquad (1)$$

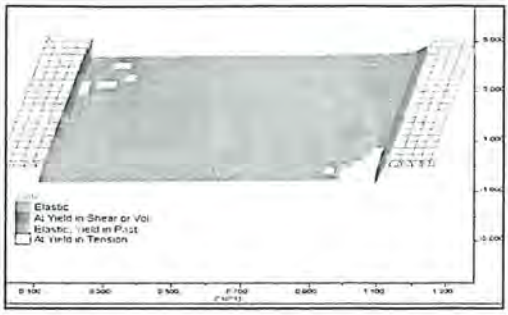

Figure 4. Sill mat sliding failure mode – plasticity state.

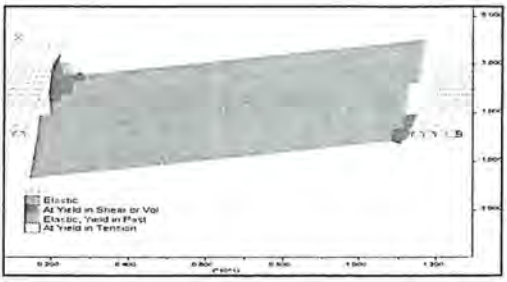

Figure 5. Sill mat rotational crushing failure mode – plasticity state.

- σ_t = tensile strength of CRF (kg/m*s^2);
- τ_t = shear strength of CRF (kg/m*s^2);
- σ_c = horizontal confining stress (kg/m*s^2);
- γ = unit weight of the material (kg/m^2*s^2);
- L = stope span (m);
- d = sill depth (m);
- β = inclination of stope (°);

5.2 *Sliding failure*

Figure 4 illustrates sliding failure of a sill mat. The hangingwall and footwall sill-host rock contact fails in shear.

$$(\sigma_v+d\cdot\gamma) > 2\cdot\left(\frac{\tau_t}{\sin^2(\beta)}\right)\cdot\left(\frac{d}{L}\right) \qquad (2)$$

5.3 *Rotational – crushing failure*

Rotational-crushing failure (Fig. 5) illustrates that failure occurs when the sill in contact with the hangingwall crushes (i.e., fails in compression) as the sill mat rotates. Tensile failure of the footwall/sill contact results in the rotation of the sill with respect to the bottom footwall/sill contact. These failures must occur simultaneously in both the hangingwall and the footwall.

$$(\sigma_v+d\cdot\gamma) > \frac{d^2\cdot\sigma_t}{L\cdot(L-d\cdot\cot(\beta))\cdot\sin^2(\beta)} \qquad (3)$$

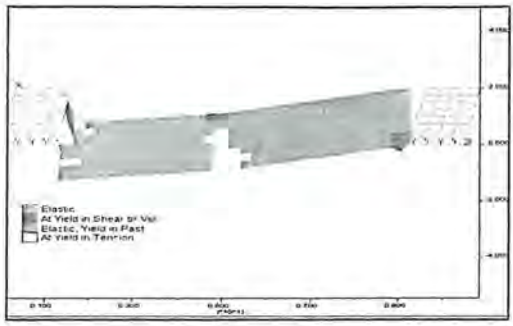

Figure 6. Sill mat rotational breaking failure mode – plasticity state.

5.4 *Rotational – breaking failure*

A similar result occurs in the rotational-breaking failure mode (Fig. 6), where the centrifuge model (Mitchell 1991) predicts that a tensile failure propagates at the same angle as the dip of the stope, rotating about point "O". Numerical modeling predicts that this failure occurs at approximately mid-span, with no particular angle of failure. The numerical solution implies that failure occurs where the sill, in contact with the hangingwall, crushes (i.e., fails in compression), as the sill mat rotates and breaks.

6 ANALYTICAL EQUATION CONSIDERING SHEAR STRENGTH ON HANGINGWALL

The original rotational analytical formulation was derived by Mitchell. The following analytical formulation incorporates shearing resistance at the hangingwall contact surface. Safety considerations demand conservative estimation so that, in this particular case, only some extent of the shearing resistance should be taken into account. This approach suggests that, for the sill mat rotational failure mode, shear strength should be considered a component of the analytical solution derived by Mitchell.

A multiplier factor, α, ranging from 0 to 1, is added to the equation, corresponding to either the estimated contact length at the hangingwall between the rock wall and the cemented rockfill material or the quality of the contact, absent in the original equation. After careful inspection, if it is determined that there is poor quality contact between the rock wall and the CRF, then an α equal to zero should be used, yielding Mitchell's result which is in turn more conservative.

The following equation can still be considered conservative given that sill mat failure (when a circular shear failure occurs) produces additional shearing resistance as the pillar slides against the rock wall (τ_t), as shown in Figure 7.

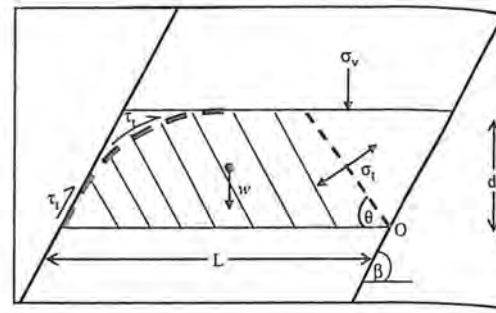

Figure 7. Rotational failure considering shear strength in the hangingwall of the sill mat.

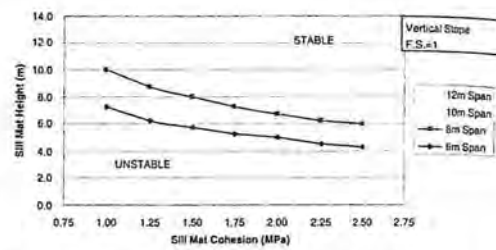

Figure 8. Sill mat stability for stope dipping at 90° – No strength on HW ($\tau_t = 0\%$) – Analytical Solution.

$$(\sigma_v + d \cdot \gamma) > \frac{\sigma_t \cdot d^2 + \alpha \cdot 2 \cdot \tau_t \cdot d \cdot L \cdot \sin^2(\beta)}{L \cdot (L - d \cdot \cot(\beta)) \cdot \sin^2(\beta)} \quad (4)$$

Also, tensile failure could occur at an angle differing from θ and a location differing from point "O", as predicted by numerical modeling.

7 SILL MAT DESIGN CURVES

Figures 8 to 11 represent a series of design curves that predict the point of failure for a given strength in term of cohesion and sill mat geometry in terms of sill height and stope span. In each graph, the y-axis (in meters) represents the minimum height, or sill thickness of a CRF sill mat necessary to be in a stable state. The graphs are of two types: no strength on hangingwall contact and 100% strength on hangingwall contact, as corresponding to the percentage of the CRF cohesion value.

The individual curves within each graph represent specific stope spans, ranging from 6 meters to 12 meters. All cases assume uniform vertical stress acting on the top of the CRF sill mat. A stable CRF sill mat is represented as being anywhere above the individual design curve in question (e.g., 6, 8, 10, or 12 meter span), implying a safety factor of 1.0 or greater.

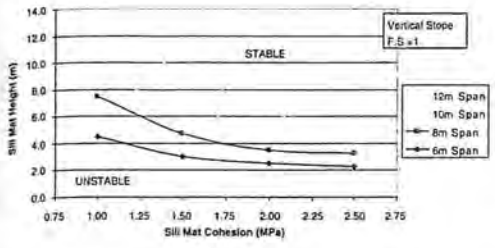

Figure 9. Sill mat stability for stope dipping at 90° – No strength on HW ($\tau_i = 0\%$) – Numerical Solution.

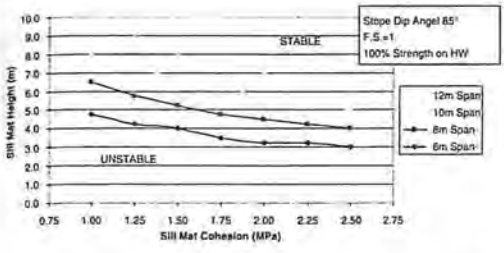

Figure 10. Sill mat stability for stope dipping at 85° – 100% strength on HW ($\tau_i = 100\%$) – Analytical Solution.

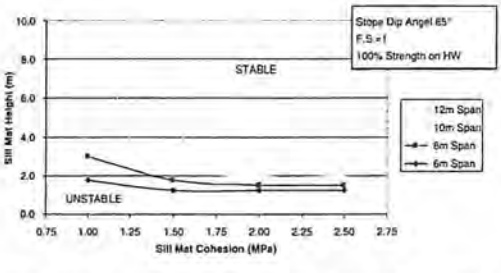

Figure 11. Sill mat stability for stope dipping at 85° – 100% strength on HW ($\tau_i = 100\%$) – Numerical Solution.

Figures 8 and 10 were obtained using numerical modeling whereas Figures 9 and 11 were obtained using the analytical equations presented above. Each point of the analytical derived curves is determined when all the three factors of safety that represent each failure mode is at least 1.0, in other words, the sill mat height that yields all three factors of safety equal or greater than 1.0 is the one selected.

These design curves enables the operator to select the sill dimensions, given the cohesive strength of the fill material, and the parameters considered of greatest significance to the design such as:

- span;
- wall dip; and
- HW shear strength.

The *Flac*^{2D} approach used in this study does not incorporate a factor of safety in its method of design. However, by applying a factor of safety to the cohesion parameter, the total factor of safety in the overall design will be improved.

8 CONCLUSIONS

The existing analytical equation for the rotational failure mode does not consider shear strength on hangingwall/sill mat contact, due to the low strength of pastefill and/or the gap that may occur at the contact surface (as a result of low dip angle), given the method of pastefill delivery itself (i.e., via piping), and so it becomes difficult to maintain firm contact. Methods of constructing sill mat pillars employing rockfill most likely can overcome this problem, in nearly all cases, and so a new analytical equation that considers shear strength of the wall contact is presented. As a result of this new analytical equation, there is a significant increase in the factor of safety of a given sill mat.

Although analytical equations are useful in the design of sill mat pillars, the author considers that numerical modeling is a more accurate method of designing sill mat pillars given numerical modeling's capacity of incorporating several additional factors that influence stability. These factors include: material deformation, and the reduction in strength properties throughout the modeling process (as a function of the strain on grid elements). Among the strategies assessed, the finite difference program *Flac*^{2D} was considered to be the most suitable program in addressing and understanding the mechanics of the various failure modes of cemented rockfill sill mats, and the parameters involved in rockfill sill mat design.

Design curves for the stability of cemented rockfill sill mats were developed to aid in the design of new pillars or to reassess the performance of existing pillars at different mining operations. It is imperative that, when mining under backfill, no personnel are exposed to the danger, and remote mining methods are employed (with a minimum factor of safety of 1.2 for non-entry methods). This is the lowest useable factor of safety to ensure that the sill mat remains integral during its exposure. The above statement notwithstanding, via numerical modeling it was only determine sill mat pillar stability with a factor of safety of 1.0, and by incorporating a suitable factor of safety on the input strength parameters (cohesion) the operator is able to produce a design within existing construction guidelines.

The rotational failure mode obtained via numerical modeling differs from that obtained in previous existing research employing centrifuge models. Two rotational failure modes were generated via numerical modeling, rotational-crushing and rotational-breaking. Neither implied tensile failure at the footwall propagating at an angle of the same magnitude as the stope dip angle, but in a direction defined by the

supplementary angle, as predicted by Mitchell's rotational failure mode equation. Rotational-crushing failure mode predicts tensile failure at the footwall contact and shear (or volumetric) failure at the hangingwall contact, whereas the rotational-breaking failure mode predicts a tensile failure propagating vertically at mid-span, and a shear (or volumetric) failure at the hangingwall contact.

REFERENCES

Swan, G. & Brummer, R.K. 2001. Backfill design for deep, underhand drift-and-fill mining. In *Proceedings of the 7th International Symposium of Mining with Backfill.*

Mitchell, R.J. 1991. Sill mat evaluation using centrifuge models. *Mining Science and Technology* 13: 301–313.